PHYSICAL REVIEW B **90**, 081107(R) (2014)

Kondo scattering in δ-doped $LaTiO_3/SrTiO_3$ interfaces: Renormalization by spin-orbit interactions

Shubhankar Das,[1] A. Rastogi,[1] Lijun Wu,[2] Jin-Cheng Zheng,[3] Z. Hossain,[1] Yimei Zhu,[2] and R. C. Budhani[1,4,*]
[1] *Condensed Matter–Low Dimensional Systems Laboratory, Department of Physics, Indian Institute of Technology, Kanpur 208016, India*
[2] *Condensed Matter Physics and Material Science Department, Brookhaven National Laboratory, Upton, New York 11973, USA*
[3] *Department of Physics and Fujian Provincial Key Laboratory of Theoretical and Computational Chemistry, Xiamen University, Xiamen 361005, China*
[4] *National Physical Laboratory, Council of Scientific and Industrial Research, New Delhi 110012, India*
(Received 17 February 2014; revised manuscript received 30 July 2014; published 13 August 2014)

We present a study of δ doping at the $LaTiO_3/SrTiO_3$ interface with isostructural antiferromagnetic perovskite $LaCrO_3$ that dramatically alters the properties of the two-dimensional electron gas at the interface. The effects include a reduction in sheet-carrier density, prominence of the low-temperature resistivity minimum, enhancement of weak antilocalization below 10 K, and observation of a strong anisotropic magnetoresistance (MR). The positive and negative MR for out-of-plane and in-plane fields, respectively, and the field and temperature dependencies of MR suggest Kondo scattering by localized Ti^{3+} moments renormalized by spin-orbit interaction at T < 10 K, with the increased δ-layer thickness. Electron-energy-loss spectroscopy and density functional calculations provide convincing evidence of blocking of electron transfer from LTO to STO by the δ layer.

DOI: 10.1103/PhysRevB.90.081107 PACS number(s): 73.20.−r, 68.55.Ln, 72.15.Gd, 72.15.Qm

The phenomenon of the formation of a two-dimensional electron gas (2DEG) at the interface of epitaxially grown $LaTiO_3$ (LTO) or $LaAlO_3$ (LAO) on TiO_2-terminated $SrTiO_3$ (STO) [1–3] has attracted much attention in recent years [4–9]. It is generally agreed that the gas is formed by the transfer of electrons from the polar layer of LAO or LTO to the top TiO_2 layer of STO. Since the carrier concentrations $n_\square$ are large ($\sim 3 \times 10^{14}/\mathrm{cm}^2$) and some of the Ti^{4+} ions at the interface may also get converted to Ti^{3+} with $S = 1/2$ localized spin, the electron dynamics is likely to be controlled by weak electron-electron (e-e) scattering and magnetic scattering in addition to the effects of weak static disorder. Moreover, as the interface breaks inversion symmetry, there is a possibility of Rashba spin-orbit scattering [10] emanating from the interface electric field. Some of these issues have been addressed by measuring the magnetoresistance (MR) of 2DEG formed at LAO/STO [11–13] and electrolyte-gated STO [14]. However, no consensus has emerged on the origin of a strong positive MR observed when the external magnetic field is perpendicular to the plane of the film ($H_\perp$), the change in the sign of the MR when the field is brought in the plane ($H_\parallel$), the characteristic minimum in $R(T)$ below $\sim$100 K followed by $\ln T$ behavior, and, finally, the saturation of $R(T)$ at still lower temperatures.

In order to address the mechanism of 2DEG formation at the LTO/STO interface and to identify the dominant scattering processes that control the nature of MR in this system, we have used the approach of δ doping of the interface. The doped structure consists of LTO[m unit cell (uc)]/LCO(δ uc)/TiO_2 terminated STO. $LaCrO_3$ (LCO)/STO alone does not form a 2D gas. The LCO film remains an antiferromagnetic insulator with a Cr site spin of 3/2 and $T_N = 298$ K. This is interesting because Cr follows vanadium in the 3d transition series and the $LaVO_3/SrTiO_3$ interface is conducting [15]. However, when LCO is inserted as a δ layer, the 2DEG nature of LTO/STO is retained for smaller values of δ (<3), but with increasing δ, a significant blocking of carriers by LCO makes the interface insulating. The temperature, magnetic field, and angular dependence of MR in $\delta = 0$ indicate a dominant Kondo-type s-d scattering for the $H_\parallel$ field. However, the Kondo's characteristic negative MR is superseded by positive MR resulting, presumably, from the enhanced forward scattering of diffusive electrons by the spin-orbit (S-O) interaction in the $T \leq 10$ K regime. For $H_\perp$, the classical positive MR quadratic in the field is seen at $T > 10$ K. It is interesting to note that the Rashba coupling at the interface of LTO/STO can be modulated by insertion of LCO layers.

The films are deposited using pulsed laser ablation on STO, as described in our earlier works [3,16]. We have deposited three sets of films. In the first set 0, 0.5, 3, 5, and 10 uc of LCO were grown on STO, followed by a 20-uc-thick LTO film. In the second set the δ is 5 uc, and the LTO was varied from 4 to 24 uc. In the last set, the LTO is 16 uc, while LCO was reduced from 5 to 0 uc in steps of 1 uc. The atomic and chemical states of the interface have been studied using x-ray reflectivity and cross-sectional scanning transmission electron microscopy (STEM) in conjunction with electron-energy-loss spectroscopy (EELS). In addition, density functional theory (DFT) calculations have been performed to analyze the charge-density profile of the interface. Electron transport measurements have been performed in a 14-T system (Quantum Design PPMS) fitted with a sample rotator which allowed measurement of angular MR.

Figure 1 shows a sketch of various atomic planes of the heterostructure along with high-angle angular-dark-field (HAADF) images taken from STEM. The atomically sharp interfaces and uniformly distributed 3-uc LCO between LTO and STO are clearly seen with the bright background contrast due to the high atomic number Z in the LCO unit cell. The peak intensity marked by the red arrows in Fig. 1(d), which is higher than the average Sr peak in STO, indicates diffusion of La/Cr into STO, limited to 1 to 2 uc. A 2D elemental map based on the EELS spectrum image shown in Fig. S1 of the Supplemental Material [17] also confirms the coherent and atomic sharp interfaces. An EELS image with the Ti $L_{2,3}$, O K, and Cr $L_{2,3}$

*rcb@iitk.ac.in, rcb@nplindia.org

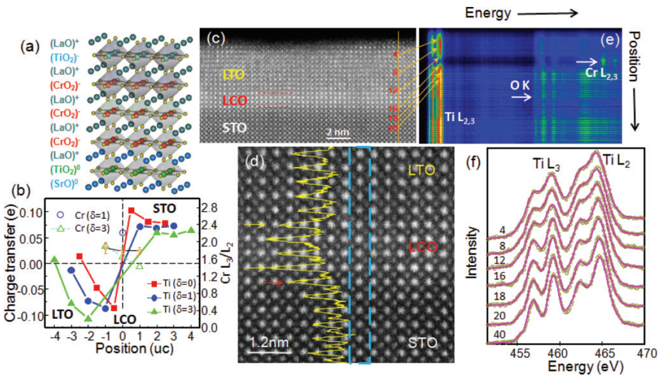

FIG. 1. (Color online) (a) Oxide planes along the [001] direction of the δ-doped interface. (b) DFT charge transfer in $(LTO)_3(LCO)_\delta(STO)_3$. The positive (negative) value indicates the gain (loss) of the charge. The left, middle, and right regions are 3 uc of LTO, δ uc of LCO, and 3 uc of STO, respectively. This plot also shows the Cr L_3/L_2 intensity ratio across the interface (brown inverted triangles). (c) and (d) HAADF image showing interfaces between LTO, LCO, and STO with 3-uc LCO (bright atom columns). An intensity line profile (yellow) from the column marked by the dark blue line is included in (d). (e) EELS spectrum image from the vertical scan line in (c), showing Ti $L_{2,3}$, O K, and Cr $L_{2,3}$ edges at ≈460, 530, and 580 eV, respectively. (f) A series of Ti $L_{2,3}$ edges (circles) across two interfaces from the spectrum image (e) acquired from the line scan partially shown in (c) (see text for details).

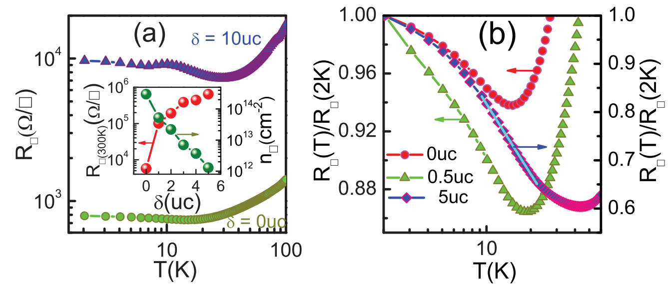

FIG. 2. (Color online) (a) Temperature dependence of $R_\square$ of LTO(20 uc)/LCO(δ uc)/STO heterostructure. The inset shows the variation of $R_\square$ and $n_\square$ with doping in LTO(16 uc)/LCO(δ uc)/STO. (b) $R_\square(T)/R_\square(2\text{ K})$ of $\delta = 0$, 0.5 and 5 uc. The solid line in $\delta = 5$ uc curve is the ln T fit.

edges from the vertical scan line in Fig. 1(c) extended into STO is depicted in Fig. 1(e). The EELS spectra (circles) as a function of atomic position [Fig. 1(c)] are plotted in Fig. 1(f). The overlaid red lines are the results from the multiple linear least-squares fitting, the spectrum with the weighted linear combination of Ti^{3+} and Ti^{4+} reference spectra. Four distinct peaks representing the e_g and t_{2g} electron orbitals of the Ti L_2 and L_3 energy levels are clearly visible on the STO side, and they became broader with peak separation of e_g and t_{2g} and are less pronounced at the interface and into the LTO side, indicating an increase of the Ti^{3+} state. Composition mapping revealed a constant distribution of oxygen across the region and a complementary increase and decrease in Cr and Ti, respectively, in the LCO layer with a 1–2-uc diffusion length [17]. Since it is known that the Cr^{2+}-containing compounds have a higher L_3/L_2 Cr-absorption edge intensity ratio compared to the Cr^{3+}-containing compounds [18,19], we have analyzed the L_3 and L_2 intensities for $\delta = 1$, 2, and 3 uc samples (see Fig. S7 of the Supplemental Material). Our analysis indicates that L_3/L_2 changes from 1.84 to 1.77 on moving from the LTO/LCO interface to the LCO/STO interface in the $\delta = 3$ uc sample. This result suggests that the δ layer gains electrons from the LTO layer. The percentage of Ti^{3+} over the sum of Ti^{3+} and Ti^{4+} across the interface suggests a significant charge transfer from LTO to STO near the interface. To confirm these findings, we conducted DFT calculations by constructing a supercell with 3-uc LTO on the left, δ-uc LCO in the middle, and 3-uc STO on the right [17]. The calculations show significant charge transfer from LTO to STO [Fig. 1(b)], which reduces with the increase of δ. Interestingly, Cr in LCO also receives electrons, confirming its reduced valence state as suggested by EELS measurements.

Figure 2(a) shows the sheet resistance $R_\square$ as a function of temperature T for LTO(20 uc)/LCO(δ uc)/STO samples of $\delta = 0$ and 10. We see a metallic behavior upon decreasing T from 300 K. On cooling below ≈20 K, a resistance minimum followed by a slight upturn and then saturation of $R_\square$ at $T \leq 7$ K is seen for $\delta = 0$. As the δ layer becomes thicker, the minimum T_m shifts towards higher temperature, and the upturn becomes more prominent. This trend in $R_\square$ was seen in all samples of $\delta = 0.5$, 3, 5, and 10 uc. The inset of Fig. 2 (a) shows $R_\square$ and $n_\square$ at 300 K as a function of δ-layer thickness. While $R_\square$ increases progressively, $n_\square$ decreases with the increase in the δ layers. For $\delta = 0$, $n_\square$ at 300 K is $\approx 3 \times 10^{14}$ cm^{-2}, which is very close to the areal charge density (3.2×10^{14} cm^{-2}) expected if half an electron per unit cell is transferred to the STO surface from the LTO layers to suppress the polarization catastrophe. The insertion of a few unit cells of LCO leads to a dramatic decrease in $n_\square$, by a factor of 50 and 280 for $\delta = 3$ uc and $\delta = 5$ uc, respectively, at 300 K. These observations are consistent with STEM results, which suggest conversion of Cr^{3+} to Cr^{2+} in the LCO layers, and the results of the DFT calculations.

Figure 2(b) is a plot of $R_\square(T)/R_\square(2\text{ K})$ of $\delta = 0$, 0.5, and 5 uc to emphasize the minimum in $R_\square(T)$ at T_m. Below T_m the resistance follows a $\ln T$ dependence, but this divergence is cut off on further decreasing the temperature. This saturating tendency of $R_\square$ is prominent in $\delta = 0$. The simplest interpretation for the $\ln T$ rise can be given in terms of weak localization (WL) in 2D where a constructive interference between partial waves of diffusive electrons can lead to enhanced backscattering and hence an increase in resistance, which continues to grow at lower temperatures as the dephasing inelastic scattering is reduced due to phonon freeze-out [20,21]. Since weak localization is an orbital effect, it has a distinct dependence on the angle between H and the plane of the film. $H_\perp$ quenches quantum backscattering because of the Aharonov-Bohm phase acquired by the partial waves. A similar dependence of $R_\square$ in zero field also results from the e-e interaction in 2D [22,23]. The distinction between the two can be made by measuring the MR, which in the latter case is positive and mostly isotropic. However, before we dwell upon the MR data, a key observation of Fig. 2(b) is the truncation of the divergence of $R_\square$ at $T \ll T_m$. Such an effect can arise due to a phenomenon closely associated with WL in the presence of the S-O interaction. The dephasing of the spin degree of freedom by S-O in diffusive trajectories can suppress the quantum backscattering and thereby truncate the $\ln T$ growth of $R_\square$ at low temperatures. This weak antilocalization (WAL) [20] becomes prominent at $T \ll T_m$ as the S-O gains strength at lower temperatures.

Here it is pertinent to introduce one more scattering phenomenon which can lead to a minimum followed by saturation of $R_\square$ in disordered metallic films. This is the Kondo scattering of conduction electrons of spin $\overrightarrow{S_e}$ by a localized magnetic impurity in a system of spin $\overrightarrow{S_i}$. The interaction between the two moments is given by the Hamiltonian $H_{ex} = J \cdot \overrightarrow{S_i} \cdot \overrightarrow{S_e}$, where J is positive, and hence a stable configuration demands antiparallel arrangement of $\overrightarrow{S_i}$ and $\overrightarrow{S_e}$. The Kondo interaction leads to a resistivity $\Delta\rho_k = -B \ln T$, where B is a positive constant and a function of J, $N(E_F)$ (the density of states at the Fermi level), and other properties of the electron gas. However, $\Delta\rho_k$ cannot increase without a bound [24]. Eventually, the divergence of $\Delta\rho_k$ is cut off, and it becomes constant below a temperature of the order of the Kondo temperature, $T_K = T_F \exp(-1/JN)$. This unitary limit is, however, not reached in metal films [25–27]. An H field suppresses Kondo scattering, thereby leading to a negative isotropic MR. Recently, a Kondo mechanism has been proposed for $R_\square(T,H)$ of a 2DEG formed on the surface of STO by electrostatic gating [14]. It has been argued that highly localized $3d^1$ electrons of some Ti^{3+} ions (spin 1/2) are the source of Kondo scattering. The idea of magnetic scattering is supported by the recent observation of ferromagnetism at the LAO/STO interface [7].

In Fig. 3 we show $R_\square(T)$ at different $H_\perp$ for $\delta = 0$, 0.5, 3, and 5 uc. $H_\perp$ shifts the resistivity minimum to higher T (see insets), and a dramatic positive MR is evident which is inconsistent with the WL but agrees broadly with the e-e scattering scenario. In the latter case the magnetoconductance increases as $\sim -\frac{e^2}{\hbar}\frac{\tilde{F}_\sigma}{4\pi^2}(0.084)(\frac{g\mu_B H}{k_B T})^2$ for $\frac{g\mu_B H}{k_B T} \ll 1$, where $\tilde{F}_\sigma$ has an upper bound of 4/3. Clearly, a positive MR is expected which increases as H^2. At high field a $\ln(H)$ dependence of MR has been predicted.

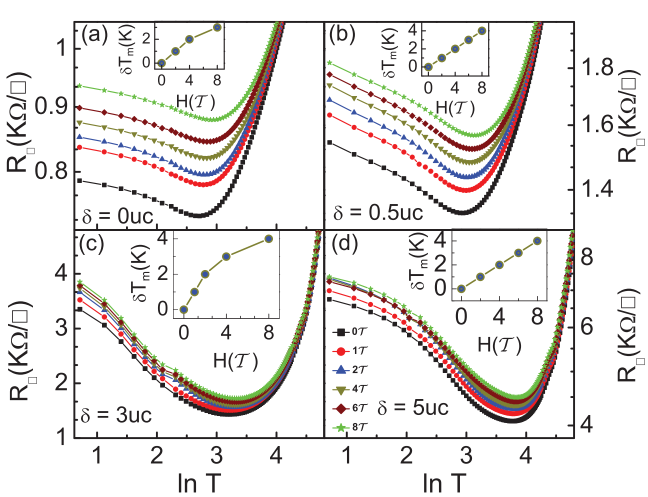

FIG. 3. (Color online) (a)–(d) $R_\square(T)$ of LTO(20 uc)/LCO(δ uc)/STO films as a function of $\ln T$ for different $H_\perp$. The inset shows δT_m vs $H_\perp$, where $\delta T_m = T_m(H) - T_m(0)$. All the samples show positive MR down to 2 K.

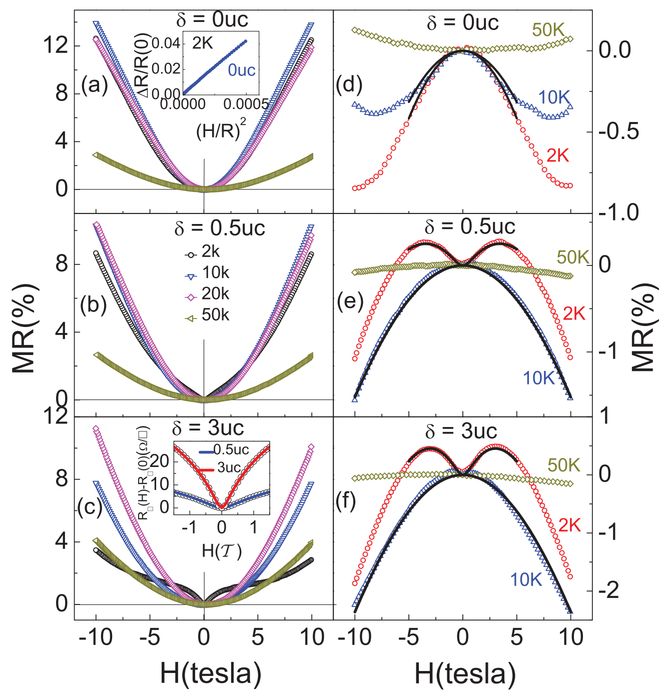

FIG. 4. (Color online) (a)–(c) $MR_\perp$ of $\delta = 0$, 0.5, and 3 uc, respectively. The inset in (a) shows a Kohler plot for $\delta = 0$ uc, while the inset in (c) reveals the WAL effect after subtracting high-field H^2 data. The solid curves in the inset in (c) are the fit to the Eq. (1). (d)–(f) $MR_\parallel$ for the same set of samples. A negative $MR_\parallel$ for all three temperatures is seen for $\delta = 0$, but $\delta = 0.5$ and 3 uc show positive $MR_\parallel$ at lower field at 2 K and a crossover from positive to negative MR at higher field. In (e) and (f) the black solid line for the 10 K $MR_\parallel$ is the fit using the Kondo model [Eq. (2)], and at 2 K it is fitted using Kondo + WAL in the range -5 T $\le H \le 5$ T.

We probe the MR further as a function of H field. A positive ($\approx$14%) out-of-plane MR ($MR_\perp$) for $\delta = 0$ uc is observed at 2 K and 10 T [Fig. 4(a)]. The $MR_\perp$ has an H^2 dependence, which, at first glance, can be attributed to the e-e scattering. The upper bound for H to have an H^2 dependence at 4.2 K is $\approx$3.16 T, and the slope of the MR vs H^2 curve is $\approx 0.714 \times 10^{-7}/T^2$ (calculated from the e-e scattering theory). However, the measured slope for $\delta = 0$ is $1.69 \times 10^{-3}/T^2$, which suggests that the e-e interaction alone is not responsible for the large $MR_\perp$. A sizable contribution to $MR_\perp$ can also come from the classical defect scattering [28] that follows Kohler's rule: $\frac{\Delta R}{R_0} \propto a[\frac{H}{R_0}]^2$. The inset of Fig. 4(a) shows a Kohler plot for $\delta = 0$. From these $MR_\perp$ data the mobility of carriers at 2 and 100 K turns out to be 403 and 86 $cm^2\ V^{-1}\ S^{-1}$, respectively.

Figures 4(b) and 4(c) show that the $MR_\perp$ at 2 K and 10 T for $\delta = 0.5$ and 3 uc decreases to 9% and 4%, respectively. At lower fields it also deviates from H^2, and a cusp appears near $H = 0$. This indicates the presence of an additional scattering mechanism that becomes operational below $\approx$10 K. We separate out the contribution of this process by extrapolating the H^2dependence seen at $H \ge 6$ T to lower fields and then subtracting the extrapolated value from the measured $R_\square(H)$

[inset of Fig. 4(c) for $\delta = 0.5$ and 3 uc]. We attribute this distinct contribution to $MR_\perp$ at $T \leq 10$ K to S-O scattering, which, in the 2D limit for $H_\perp$, can be expressed as [21,22,29,30]

$$\frac{\Delta R_\square(H)}{[R_\square(0)]^2} = -\frac{e^2}{2\pi^2\hbar}\left[\Psi\left(\frac{1}{2}+\frac{H_\varphi}{H}\right) - \ln\frac{H_\varphi}{H}\right], \quad (1)$$

where $\Delta R_\square(H) = R_\square(H) - R_\square(0)$, $\Psi(x)$ is the digamma function, and $H_\varphi = \hbar/(4eL_\varphi^2)$. The length $L_\varphi = \sqrt{D\tau_\varphi}$, where D and τ_φ are the diffusion constant and phase coherence time, respectively. The inset of Fig. 4(c) shows the fits of Eq. (1) to $MR_\perp$ of $\delta = 0.5$ and 3 uc. This yields $L_\varphi \approx 33$ and 46 nm for $\delta = 0.5$ and 3 uc, respectively. These numbers are reasonable considering that the scattering is taking place in the plane of the film where L_φ has no dimensional constraints.

Figures 4(d)–4(f) show $MR_\parallel$ of $\delta = 0$, 0.5, and 3 uc films. Interestingly, for $\delta = 0$ we have a negative $MR_\parallel$ at $T < 50$ K. The suppression of classical positive MR can be understood as resulting from the thickness of the 2DEG being within one carrier mean free path. This MR anisotropy also supports the 2D nature of the metallic state in these interfaces.

Interesting values of $MR_\parallel$ are seen in Figs. 4(e) and 4(f) for $\delta = 0.5$ and 3 uc, respectively, at 2 K. Here, the data can be divided in two regions, a positively sloped MR at lower field and a negatively sloped MR at higher field, resulting in a local MR maximum seen at 3.6 and 3.2 T for $\delta = 0.5$ and 3 uc, respectively. In our samples these maxima are observed at a much higher field than in 2D metal films of Bi and Au, where the crossover fields are ∼0.1 and 2.5 T, respectively [11,31,32]. This in-plane positive $MR_\parallel$ diminishes above ∼5 K.

The negative $MR_\parallel$ supports the Kondo mechanism. To establish this idea further, we fit the $MR_\parallel$ of $\delta = 0$, 0.5, and 3 uc at 10 K to a simple Kondo model [14],

$$R^{\text{model}}(H_\parallel) = R_0 + R_K(H_\parallel/H_1), \quad (2)$$

where R_0 is the residual resistance, $R_K(H_\parallel/H_1)$ is a function of the zero-temperature MR of Kondo impurity, which is related to magnetization and can be calculated using the Bethe-ansatz technique [17], and H_1 is an H-field scale related to T_K and the g factor of the impurity spin [33]. The $MR_\parallel$ at 2 K for $\delta = 0$ uc also fits to the Kondo model [Eq. (2)]. We note that the negative $MR_\parallel$ at 10 T [Figs. 4(e) and 4(f)] increases with δ-layer thickness and thus bears an inverse relation to $n_\square$ [see Fig. 2(a)]. In Kondo's theory $R_K(T=0,H=0) \propto n_\square^{-1}N(E_F)^{-1}$ [34]. The data shown in Figs. 4(e) and 4(f) are consistent with this picture.

The positive $MR_\parallel$ at 2 K for $\delta \neq 0$ at fields below the critical value appears to be the contribution of the WAL. To fit the 2 K data we add the WAL and Kondo terms [Eqs. (1) and (2)]. As the WAL effect is insignificant at higher fields, we fit the 2 K data in the range $-5\text{ T} \leq H \leq 5$ T. The black line in Figs. 4(e) and 4(f) for the 2 K data is this fit [17]. The quality of the fit strongly suggests that the WAL effect overrides the Kondo scattering at $T < 10$ K.

The MR for $\delta = 0$, 0.5 and 3 uc for different orientations θ of H with respect to the sample normal has been measured (see Fig. S6 in the Supplemental Material). As we tilt H towards the sample plane, a crossover from positive MR to negative MR is observed. This change in sign at 10 T happens at 80°, 70° and 50° for $\delta = 0$, 0.5, and 3 uc, respectively. The angular variation of $R_\square$ is of the type $R(\theta,T) = R(T)\cos^2(\theta) + R_0(T)$, where $R(T = 2\text{ K}) = 33$, 36, 44 Ω and $R_0(T = 2\text{ K}) = 233$, 466, 906 Ω for $\delta = 0$, 0.5, 3 uc, respectively.

In summary, we have established a strong suppression of $n_\square$ in a 2DEG at the LTO/STO interface by inserting a δ-thick layer of an isostructural perovskite LCO. Our spectroscopic measurements suggest that Cr ions at the interface act as traps and absorb the electron donated by the LTO. The saturation tendency of resistance at $T \leq 10$ K and the ln T dependence between 10 K and T_m are consistent with the Kondo scattering of electrons by localized spins. The origin of the latter can be attributed to electrons in the Ti d^1 configuration which are presumably, in Ti_{xy} orbitals, forming heavy polarons with spin $S = 1/2$ while the conduction takes place in the extended band of the $Ti_{yz/zx}$ motif [14,35–37]. Such a Ti^{3+} site will presumably have zero spin due to complete delocalization of the $3d^1$ electron. We also argue that the interfacial Cr^{3+} ions ($S = 3/2$) may also contribute to s-d scattering. However, as most of the Cr^{3+} spins are antiferromagnetically ordered, such a contribution may come from only the disordered spins located at the $LaCrO_3$-$SrTiO_3$ interface. Our STEM results shown in Fig. 1(d) do indicate some diffusion of La/Cr into STO. Further, if some of the Cr^{3+} ions are converted into Cr^{2+}, as indicated by our EELS measurements and also suggested by the depletion of 2DEG carrier density on δ doping, the site spin of Cr^{3+} would deviate from $S = 3/2$ and affect the antiferromagnetic arrangement. The emergence of a cusp in the positive MR for $H_\perp$ in δ-doped samples at $T < 10$ K is in agreement with the prediction of 2D WAL theory, as shown by the large value of L_φ. The 2D WAL also couples with the Kondo MR response of the sample at $T < 10$ K and $H_\parallel \leq 3$ T. An important finding of this work is the enhanced S-O interaction in the presence of the δ layer. In the Rashba scenario, how the δ layer enhances the local electric field at the interface remains to be seen.

We thank P. C. Joshi for technical support. R.C.B. acknowledges a J. C. Bose National Fellowship from the Department of Science and Technology, India. S.D. and A.R. thank IIT Kanpur and CSIR for financial support. This research has been funded by CSIR-India and IIT Kanpur. Work at BNL was supported by the US Department of Energy, Office of Basic Energy Science, under Contract No. DE-AC02-98CH10886. J.C.Z. acknowledge the support of the NSF of China (Grant No. U1232110).

[1] A. Ohtomo, D. A. Muller, J. L. Grazul, and H. Y. Hwang, Nature (London) **419**, 378 (2002).

[2] A. Ohtomo and H. Y. Hwang, Nature (London) **427**, 423 (2004).

[3] A. Rastogi, A. K. Kushwaha, T. Shiyani, A. Gangawar, and R. C. Budhani, Adv. Mater. **22**, 4448 (2010).

[4] W. Siemons, G. Koster, H. Yamamoto, W. A. Harrison, G. Lucovsky, T. H. Geballe, D. H. A. Blank, and M. R. Beasley, Phys. Rev. Lett. **98**, 196802 (2007).

[5] D. A. Dikin, M. Mehta, C. W. Bark, C. M. Folkman, C. B. Eom, and V. Chandrasekhar, Phys. Rev. Lett. **107**, 056802 (2011).

[6] L. Li, C. Richter, J. Mannhart, and R. C. Ashoori, Nat. Phys. **7**, 762 (2011).
[7] A. Brinkman, M. Huijben, M. V. Zalk, J. Huijben, U. Zeitler, J. C. Maan, W. G. V. D. Wiel, G. Rijnders, D. H. A. Blank, and H. Hilgenkamp, Nat. Mater. **6**, 493 (2007).
[8] G. Herranz, M. Basletic, M. Bibes, C. Carretero, E. Tafra, E. Jacquet, K. Bouzehouane, C. Deranlot, A. Hamzic, J. M. Broto, A. Barthelemy, and A. Fert, Phys. Rev. Lett. **98**, 216803 (2007).
[9] J. Biscaras, N. Bergeal, A. Kushwaha, T. Wolf, A. Rastogi, R. C. Budhani, and J. Lesueur, Nat. Commun. **1**, 89 (2010).
[10] A. D. Caviglia, M. Gabay, S. Gariglio, N. Reyren, C. Cancellieri, and J.-M. Triscone, Phys. Rev. Lett. **104**, 126803 (2010).
[11] F. J. Wong, R. V. Chopdekar, and Y. Suzuki, Phys. Rev. B **82**, 165413 (2010).
[12] X. Wang, W. M. Lü, A. Annadi, Z. Q. Liu, K. Gopinadhan, S. Dhar, T. Venkatesan, and Ariando, Phys. Rev. B **84**, 075312 (2011).
[13] A. Joshua, J. Ruhman, S. Pecker, E. Altman, and S. Ilani, Proc. Natl. Acad. Sci. USA **110**, 9633 (2013).
[14] M. Lee, J. R. Williams, S. Zhang, C. D. Frisbie, and D. Goldhaber-Gordon, Phys. Rev. Lett. **107**, 256601 (2011).
[15] Y. Hotta, T. Susaki, and H. Y. Hwang, Phys. Rev. Lett. **99**, 236805 (2007).
[16] A. Rastogi, J. J. Pulikkotil, S. Auluck, Z. Hossain, and R. C. Budhani, Phys. Rev. B **86**, 075127 (2012).
[17] See Supplemental Material at http://link.aps.org/supplemental/10.1103/PhysRevB.90.081107 for details of the characterization and analysis of the data.
[18] T. L. Daulton and B. J. Little, Ultramicroscopy **106**, 561 (2006).
[19] R. Colby, L. Qiao, K. H. L. Zhang, V. Shutthanandan, J. Ciston, B. Kabius, and S. A. Chambers, Phys. Rev. B **88**, 155325 (2013).
[20] G. Bergmann, Phys. Rep. **107**, 1 (1984).
[21] P. A. Lee and T. V. Ramakrishnan, Rev. Mod. Phys. **57**, 287 (1985).
[22] S. P. Chiu and J. J. Lin, Phys. Rev. B **87**, 035122 (2013).
[23] M. Liu, C.-Z. Chang, Z. Zhang, Y. Zhang, W. Ruan, K. He, L. Wang, X. Chen, J.-F. Jia, S.-C. Zhang, Q.-K. Xue, X. Ma, and Y. Wang, Phys. Rev. B **83**, 165440 (2011).
[24] J. Kondo, Prog. Theor. Phys. **32**, 37 (1964).
[25] V. Chandrasekhar, P. Santhanam, N. A. Penebre, R. A. Webb, H. Vloeberghs, C. V. Haesendonck, and Y. Bruynseraede, Phys. Rev. Lett. **72**, 2053 (1994).
[26] N. Giordano, Phys. Rev. B **53**, 2487 (1996).
[27] T. Gang, M. Deniz Yilmaz, D. Atac, S. K. Bose, E. Strambini, A. H. Velders, M. P. de Jong, J. Huskens, and W. G. van der Wiel, Nat. Nanotechnol. **7**, 232 (2012).
[28] O. N. Tufte and E. L. Stelzer, Phys. Rev. **173**, 775 (1968).
[29] S. Hikami, A. I. Larkin, and Y. Nagaoka, Prog. Theor. Phys. **63**, 707 (1980).
[30] B. Grbić, R. Leturcq, T. Ihn, K. Ensslin, D. Reuter, and A. D. Wieck, Phys. Rev. B **77**, 125312 (2008).
[31] Y. F. Komnik, V. V. Andrievskii, and I. B. Berkutov, Low Temp. Phys. **33**, 79 (2007).
[32] T. Kawaguti and Y. Fujimori, J. Phys. Soc. Jpn. **52**, 722 (1983).
[33] N. Andrei, K. Furuya, and J. Lowenstein, Rev. Mod. Phys. **55**, 331 (1983).
[34] T. A. Costi, Phys. Rev. Lett. **85**, 1504 (2000).
[35] M. Salluzzo, J. C. Cezar, N. B. Brookes, V. Bisogni, G. M. De Luca, C. Richter, S. Thiel, J. Mannhart, M. Huijben, A. Brinkman, G. Rijnders, and G. Ghiringhelli, Phys. Rev. Lett. **102**, 166804 (2009).
[36] Y. Kim, R. M. Lutchyn, and C. Nayak, Phys. Rev. B **87**, 245121 (2013).
[37] B. R. K. Nanda and S. Satpathy, Phys. Rev. B **83**, 195114 (2011).